Composites: Part A 93 (2017) 199–206

Contents lists available at ScienceDirect

Composites: Part A

journal homepage: www.elsevier.com/locate/compositesa

Effect of tool surface topography on friction with carbon fibre tows for composite fabric forming

Daniel M. Mulvihill *, Michael P.F. Sutcliffe

Department of Engineering, University of Cambridge, Trumpington Street, Cambridge CB2 1PX, UK

ARTICLE INFO

Article history:
Received 5 July 2016
Received in revised form 22 September 2016
Accepted 17 October 2016
Available online 29 October 2016

Keywords:
A. Carbon fibres
A. Tow
E. Forming
Friction

ABSTRACT

The effect of tool surface roughness topography on tow-on-tool friction relevant to the dry forming of composite fabrics is investigated. A comprehensive range of tool average surface roughness R_a values from 0.005 to 3.2 μm was used in friction testing with carbon fibre tows. The measured slope of these surfaces, which is the critical surface topographical characteristic, increased significantly with increasing roughness amplitude. Friction was found to be sensitive to roughness topography for very smooth surfaces ($R_a < 0.1$ μm) and increased with decreasing roughness slope and amplitude. For rougher surfaces ($R_a > 0.1$ μm), friction was relatively insensitive to roughness slope and amplitude. A finite element idealisation of the tow-on-tool contact was used to explain these results in terms of the level of tow-tool conformance. Smooth surfaces have low slopes which allow good conformance, and hence high real contact area and friction. Rougher surfaces have high slopes, particularly at shorter wavelengths, which prevents good conformance. In this case, point contact between fibres and surface dominates, leaving the resulting friction less sensitive to roughness.

1. Introduction

Carbon fibre based composite parts are often produced by a dry fabric pre-forming stage whereby a metal tool presses carbon fabric layers into the required shape before subsequent resin infusion. Presently, the fabric forming step must be designed by an iterative process owing to the absence of a robust predictive modelling tool. Forming industry practitioners would like to be able to predict forming forces, part thicknesses, wrinkling, void formation and fabric deformation, etc., but achieving this requires a better understanding of the underlying physical phenomena in the forming process. A particular issue is the frictional behaviour both between tool and fabric and between fabric layers.

Since the carbon fibre tow is the basic building block for a fabric, recent work on friction in composites forming [1–5] has focused on tow-on-tool and tow-on-tow friction as a first step. Our own group investigated some of the fundamental mechanisms at play in Mulvihill et al. [5] (using techniques developed previously by Smerdova and Sutcliffe [6,7]). Here, it was shown for the tow-on-tool case that the 'real' fibre contact length at the tow frictional interface is not a constant following from an idealised assumption of parallel touching fibres, but increases in a characteristic repeatable manner with increasing normal load. Accounting for this evolving contact length in a Hertzian calculation of the real contact area (assuming cylindrical fibres) produced a contact area versus load variation which differed only by a constant factor compared with the measured friction force curves. The friction force curves took the form $F = kW^n$, where W is the normal load and k and n are experimentally determined constants. The exponent n was generally within the range 0.7–1. Such exponents come about due to the combination of an increasing real contact length and an increasing Hertzian contact width, in a manner analogous to the way that Greenwood and Williamson's theory [8] produces an exponent close to unity for elastically deforming rough surfaces. The constant factor between the area and friction force means that the tow behaviour agrees with the 'constant interface strength' model of friction developed by Bowden and Tabor [9], i.e. that friction force $F = \tau A$, where τ is the constant interface shear strength and A is the real contact area under the fibres (interface strength τ will clearly be related to the strength and surface energy of the sizing on the fibres). In this model the real contact area has a key role in determining the frictional behaviour. This finding can be used to explain various experimental observations. For example, Mulvihill et al. [5] and Cornelissen et al. [1] explained the higher friction measurements found for tow-on-tow contact in the parallel arrangement, as compared with the perpendicular arrangement,

* Corresponding author presently at: School of Engineering, University of Glasgow, G12 8QQ, UK.
E-mail address: daniel.mulvihill@glasgow.ac.uk (D.M. Mulvihill).

http://dx.doi.org/10.1016/j.compositesa.2016.10.017
1359-835X/

by noting that the theory predicts a smaller real contact area in the case of perpendicularly contacting tows. Likewise, the higher friction noted in [5] for the more highly sized (i.e. coated) tow was ascribed to a correspondingly higher real contact area. The number of fibres per tow was found by Chakladar et al. [4] to have little effect on the friction coefficient; presumably changing from a 6 k to a 12 k tow does not change significantly the interfacial real contact area as a fraction of the nominal contact area.

In tow-on-tool contact, another parameter which might be expected to affect frictional behaviour is that of tool surface roughness topography; this is the subject of the present paper. Roselman and Tabor [10] investigated this effect by sliding an individual carbon fibre against stainless steel counterfaces having four different roughness values (R_a = 0.01, 0.05, 0.26 and 0.95 μm). They found that friction decreases as the counterface roughness increases. The most significant decrease occurred in moving from an R_a roughness of 0.01 μm to one of 0.05 μm, while the friction difference between the rougher surfaces (from 0.05 to 0.95 μm R_a) was smaller. Cornelissen et al. [3] carried out friction measurements with carbon, E-glass, and aramid tows in contact with two steel counterfaces having R_q roughness values of 0.02 and 1.1 μm (R_a of approximately 0.018 and 1 μm). For each tow type, the smoother counterface again gave higher friction. Both Roselman and Tabor [10] and Cornelissen et al. [2] have explained this behaviour by noting that smoother surfaces should allow greater real contact area under the fibres and, hence, higher friction. They each put forward a model based on a calculation of the real contact area assuming smooth cylindrical fibres undergoing Hertzian contact with spherically tipped asperities (with constant radius) arranged on the counterface. In Roselman and Tabor [10], the asperities were simply placed along the counterface at a constant height, while Cornelissen et al. [2] gave the asperities a Gaussian distribution of heights and used a Greenwood and Williamson type analysis [8] for calculating the contact area. For their rougher surface, Cornelisson et al. [2] introduced a second scale of larger sized asperities (again with constant radius): an effective nominal contact area was first calculated based on the fibres contacting the larger sized asperities (again spherically tipped), and the Greenwood and Williamson approach was then reverted to for calculation of the real contact areas within each of these nominal contact patches. Both groups were able to use their model to show a greater real contact area for the smoother surface and thus infer a higher level of friction.

The above contact mechanics models are based on approaches from contact mechanics [11] and from Greenwood and Williamson [8] which have been used successfully for contact between hard, rigid, rough surfaces such as for the titanium alloy metal-to-metal contacts occurring in Mulvihill et al. [12,13]. However, this type of model breaks down where the ratio of true to nominal contact area is large, as can occur with soft conformal contacts. This may indeed be relevant for contact between a soft fibrous tow and a hard rough tool surface. Moreover, at small length scales the bending resistance of the fibres may become important. The assumption of Cornelisson et al. [2], that the tow fibres remain as straight cylinders as they are pushed into the distribution of asperities on the tool, may not be appropriate. These issues are explored in the paper.To understand better the problem of compliant rough contacts, it is useful to consider Westergaard's analysis [14] for a two-dimensional contact between a smooth rigid surface and a deformable surface with sinusoidal roughness, where there is a large amount of contact between the surfaces (see Johnson [11]). In this case the contact pressure $\bar{p}$ is related to the amplitude a and wavelength λ of the sinusoidal roughness by the expression:

$$\bar{p} = \frac{\pi E^* a}{\lambda} \sin^2\left(\frac{\pi A}{\lambda}\right), \tag{1}$$

where E^* is the effective contact modulus and A is the half-width of each contact patch. This result illustrates how, for a given contact area ratio $2A/\lambda$ (i.e. the ratio of the true to the nominal contact areas), the contact pressure is proportional to the ratio a/λ of the amplitude to the wavelength of the roughness. This ratio a/λ is a characteristic slope of the roughness topography. Conversely increasing a/λ results in a reduced contact area at a fixed pressure. There is a critical pressure p* given by

$$p^* = \frac{\pi E^* a}{\lambda} \tag{2}$$

above which there is complete conformance between the two surfaces, with $2A = \lambda$. More recently, Persson [15] has developed a theory for contact of soft surfaces such as rubber, to allow for different wavelengths of roughness that are present.

From this review of rough contacts it is possible to identify a number of gaps in the present understanding of the role of counterface roughness for contact of fibrous tows with rough surfaces. Firstly, only two surface roughness values were used in the only available work [3] where the effect of tool roughness in tow-on-tool friction was studied (Roselman and Tabor's work [10] was on single fibres). Therefore, there is a need for a more thorough experimental investigation. Secondly, although the models discussed above are helpful in broadly understanding the results, there are some areas of over-simplification that require improvement. One obvious (and only recently identified) over-simplification has already been mentioned: that the real fibre contact length is not a constant based on an idealised arrangement of parallel touching fibres as assumed for the model in Cornelisson et al. [2], but increases in a particular manner with normal load as described by Mulvihill et al. [5]. Another important point is that the models discussed above make no allowance for the conformance of the carbon fibres with the rough surface. The fibres are long slender cylinders which lie on a bed which is soft relative to the metal counterface, consisting of thousands of other loosely packed fibres. It is hypothesised that elastic deformation of the fibres and tows can significantly affect the conformance of the fibres with rough surfaces, hence altering the real contact area and friction. With this picture of the contact, the topographical parameter of the surface that is mostly likely to influence friction is not the roughness amplitude, but rather the characteristic slopes of the surface which will affect the conformance, as per the Westergaard model of contact. Moreover, it is likely that roughness at different length scales will have different slopes so will influence friction in different ways. The present paper undertakes a comprehensive experimental study of the effect of tool surface roughness on tow-on-tool contact by taking friction measurements with counterfaces having eight different R_a roughness values over a very wide range varying from 0.005 to 3.2 μm. A spectral analysis of the surface roughness profiles, together with a finite element contact modelling approach based on a Westergaard [14] type analysis of an soft sinusoidal surface pressed against a rigid flat, is then used to explain the friction results in terms of the degree of tow conformance with the rough surface. The critical effect of roughness slope on the conformance and friction is explored.

2. Friction measurements

2.1. Materials and methods

Tests were performed on T700SC-12k-60E carbon fibre tows (Toray Industries, Tokyo, Japan [16]), where'T700S' is the fibre type (tensile strength of 4.9 GPa), 'C' denotes that the fibres were never twisted, 12k is the fibre count and '6' gives the sizing type (in this case compatibility with epoxy). The letter 'E' corresponds to a siz-

ing of 0.3% by weight (i.e. a lightly sized tow). The average fibre diameter was measured as 7 μm in a scanning electron microscope.

During the friction test, the tow was pulled out from between two matched surfaces. Each of the eight surface pairs used had different amplitudes of surface roughness ranging from R_a values of 0.005 to 3.2 μm. Seven of the sample pairs (R_a = 0.0125, 0.025, 0.05, 0.1, 0.4, 1.6 and 3.2 μm) were produced by cutting out the roughness patches on industrial standard surface roughness comparators (Microsurf Series, Rupert and Co. Ltd., UK), as illustrated in Fig. 1. Wire electro-discharge machining was used to cut the relatively thin samples out without distortion. The 'surface ground roughness comparator' (Microsurf Series No. 315) supplied the R_a = 0.025–3.2 μm sample pairs while the 'polished surface roughness comparator' (Microsurf Series No. 336) was required for the smoother R_a = 0.0125 μm surface. These samples are made by nickel electroforming to give an accurate and reproducible surface roughness. They were chosen as the counterfaces to ensure repeatable and traceable topographies typical of ground and polished surfaces. The smoothest surface (R_a = 0.005 μm) was not available from one of the roughness comparators and hence soda lime glass was used.

The samples (measuring 21 × 13 mm) were then glued to an upper and lower plate to facilitate testing as shown in Figs. 1 and 2. Gluing was performed in a clamping apparatus with parallel upper and lower platens which ensured parallelism between the top surface of the roughness patches and the bottom surface of the plates. As shown in Fig. 2, the tow is sandwiched between the two samples during the test with the entrance edges rounded to prevent any edge effect on the friction results. The experimental rig used for testing is the same as that used in Mulvihill et al. [5]. A schematic side and plan view is given in Fig. 3. The rig allows application of normal loads W and measurement of the associated friction force F at each normal load step.

To perform the tests an appropriate length of tow was first cut from the creel. The cut was made across sections which were wrapped with masking tape so as not to interfere with the arrangement of fibres. Two additional taped sections were also created, at some distance from either side of the contact zone, to preserve the condition of the tow in the test section. The tow was then held in the double clamping fixture shown in Fig. 3 and positioned to rest on the roughness sample on the lower plate. The sample on the upper plate was balanced on top of the tow. Additional load was then applied by screwing down on four compression springs so that the spherical tips of two button load cells (fixed to transverse arms) pressed onto the surface of the cover plate. These two points of load application are equidistant on either side of the tow so that applying equal loads (determined using the load cell readout) ensures an even load with the upper plate remaining parallel to the lower plate. For each normal load step, the associated friction force was measured as the tow was pulled out by a distance of 1 mm at a constant speed (0.0066 mm/s) using a screw-driven linear stage. Most tests consisted of about 14 normal loading steps resulting in a total distance of travel of about 14 mm. A new tow specimen was not used for each normal load step as variability between sections of tow cut from the creel introduced variability into the F-W curve, thereby, somewhat obscuring the underlying behaviour associated with increasing the normal load. Instead the entire test was done by 'pulling through' the same tow specimen. After each 1 mm pull-through, the stage was stopped and the procedure repeated by further increasing the normal load. Two adjustable 'stops' were positioned against the upper plate to prevent horizontal movement during tow pull-out. The nominal length of tow in contact was 21.2 mm and the effective tow width was 7.7 mm. Note, that the tow fibre direction was perpendicular to the grinding marks (for the surface ground samples).

Normal load was recorded by summing the output from the two miniature button load cells (LBS-5, Interface Force Measurements, Arizona USA) and this load was converted to a nominal pressure p using the appropriate tow nominal contact area. Tangential force during tow pull-out was measured using a single universal tension/compression load cell (SML, 5 lb, Interface Force Measurements, Arizona, USA) mounted between the clamping fixture and the linear stage (Fig. 3). Note that the pulling force from the tow aligns with the centre of the load cell as shown by the red centreline in Fig. 3 (even though the double-clamping arrangement is offset from this centreline). The load cells were connected through a full bridge amplifier to a desktop PC via a data acquisition device (NI USB-6009) and a LabVIEW program was written to acquire and output the load data. The friction force was then extracted from the tangential force versus distance traces as the maximum value of the static friction peak (i.e. static friction). This value was halved in order to be representative of one contact surface only.

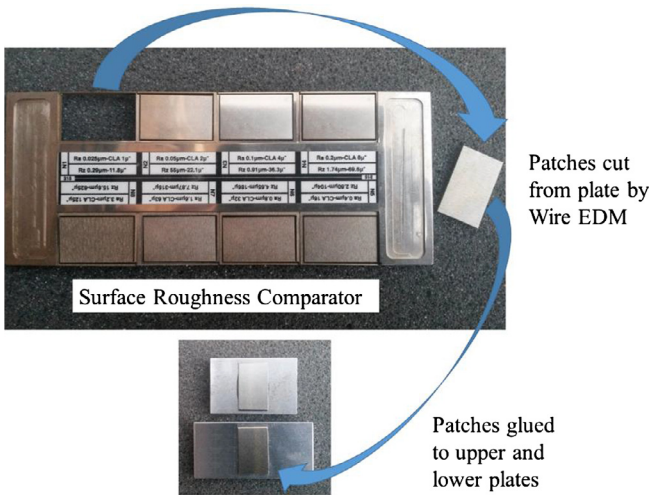

Fig. 1. Process for creating roughness samples from an industrial surface roughness comparator. Cut-out roughness patch dimensions: 21.2 × 13 mm. (For interpretation of the references to colour in this figure legend, the reader is referred to the web version of this article.)

2.2. Topography of experimental rough surfaces

This section presents a detailed analysis of the roughness present on the surfaces, using spectral analysis to understand the effect of length scale on the height and slope of the roughness present. A Taylor Hobson Form Talysurf i120 contact profilometer with a 2 μm radius diamond tip was used to measure the surface of the samples. Line profiles were taken in the direction corresponding to the tow fibre direction in the experiments. The trace length was 15 mm and the sampling interval was 0.25 μm. The raw data was imported into Matlab for spectral analysis. First form error was removed using a fourth order polynomial, then a fast-Fourier transform (FFT) implementation was used for the frequency analysis, using Welch's method of ensemble averaging to improve the quality of the spectrum (see Stoica and Moses [17]). Moreover, for the short wavelength components, frequency smoothing was used to smooth out the very dense and hence noisy spectrum. Fig. 4 plots the power spectral density for the test samples. Two repeats, taken from the top and bottom plates, are given, showing good repeatability of the spectra. There is an increase in contributions to the roughness amplitude across the frequency range with increasing sample roughness.

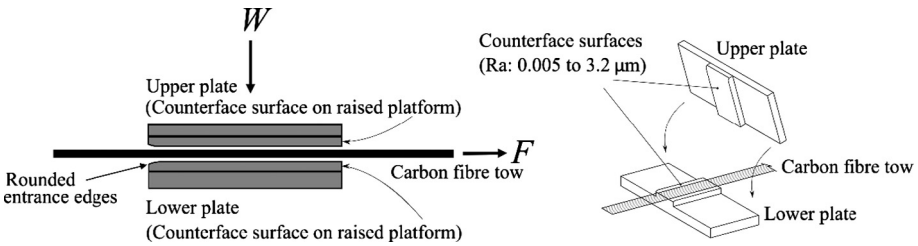

Fig. 2. Contact arrangement for tow-tool roughness testing. The tow is positioned between a pair of flat surfaces of known roughness. Normal load W is applied and friction force F is measured during tow pull-out.

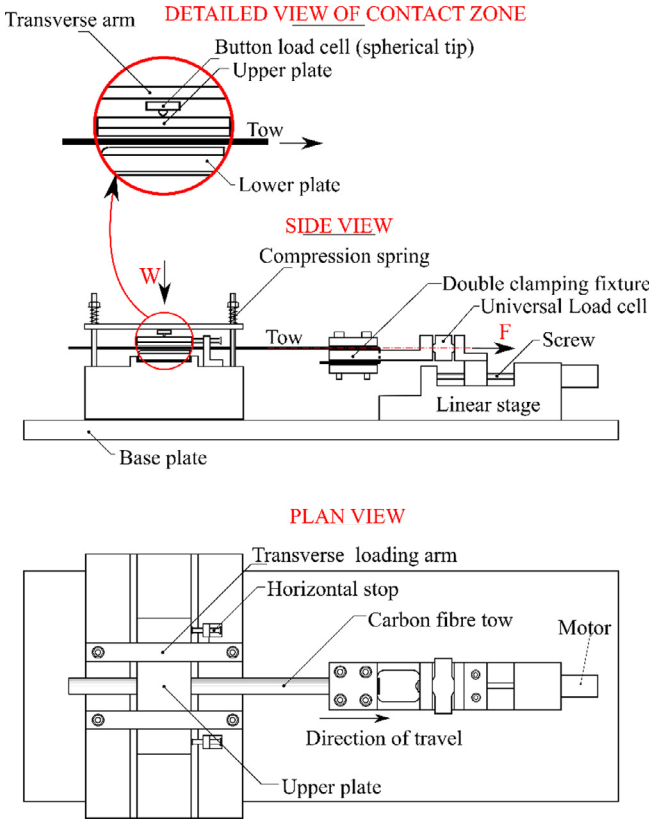

Fig. 3. Schematic diagram of experimental rig. Side view (top) and plan view (bottom). W is normal load, F is tangential load. (For interpretation of the references to colour in this figure legend, the reader is referred to the web version of this article.)

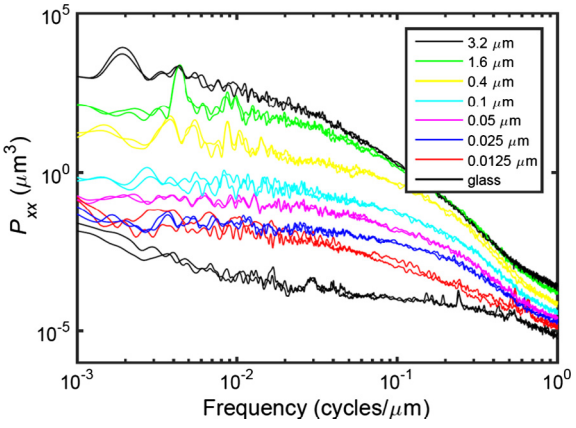

Fig. 4. Roughness power spectral density P_{xx} for the surfaces with different nominal average roughess R_a values as given in the legend. (For interpretation of the references to colour in this figure legend, the reader is referred to the web version of this article.)

The R_q roughness is given by the square root of the area under the spectrum over an appropriate range of wavelengths. Here we define the total roughness as due to all wavelengths shorter than 800 μm. The R_q roughness amplitudes associated with wavelengths of 10 and 100 μm are defined as being due to contributions from the spectrum between 3.3 and 33.3 μm for the 10 μm effective wavelength, and between 33 and 333 μm for the 100 μm wavelength. Although a rather broad-brush idealisation, this partitioning of the spectrum allows an evaluation of the effect of different wavelengths of roughness. Table 1 gives the total R_q roughness for the different samples, identified by their nominal R_a values, while Fig. 5 plots the amplitude of the roughness associated with the 10 and 100 μm wavelengths, as a function of the total R_q roughness.

Following Westergaard's theory, Eq. (1), it is expected that the ratio a/λ of the roughness amplitude to wavelength, i.e. a characteristic slope, will play an important role. The amplitude of an equivalent sinusoidal roughness was taken as equal to $1/\sqrt{2}$ times the R_q roughness from either the 10 μm or the 100 μm wavelength roughness values, as would be appropriate for a sinusoidal profile. The variation of the ratio a/λ with sample total R_q roughness is given in Fig. 6. Noting the logarithmic scales used for this plot, there is a steep rise in a/λ with increasing total R_q roughess. Moreover the roughness at a wavelength of 10 μm has a larger value of a/λ than the 100 μm wavelength roughness. Hence, we can understand that any observed changes in friction behaviour associated with the different surfaces used are likely to be due to these increases in slope which correlate with increases in roughness amplitude.

2.3. Friction results

Fig. 7 shows the friction force versus normal load plots for surface roughness R_a values between 0.005 and 1.6 μm. For clarity, the result for the roughest surface (R_a = 3.2 μm) is not shown in Fig. 7, but is included in Fig. 8 which plots the coefficient of friction $f = F/W$ against average roughness (R_a) for the final load increment of the tests (at a nominal pressure of 263 kPa). The overall trend for the tows (Fig. 8) is similar to that reported by Roselman and Tabor [10] for single fibre contact with a metal counterface; namely, that friction is not so sensitive to roughness at moderate and higher R_a values ($R_a > 0.1$), but increases markedly as the surfaces become very smooth ($R_a < 0.1$ μm). The biggest changes in friction occur between the three smoothest surfaces (i.e. 0.025 to 0.0125 to 0.005 μm); whereas, there is little change between 0.1 and 3.2 μm. There is a factor of two difference between the lowest and highest friction coefficients reported in Fig. 8. However, many engineering surfaces will lie within the range R_a = 0.1–3.2 μm where sensitivity to the roughness effect is relatively minor. The reason for the higher friction on the smoother surfaces has been

Table 1
Relationship between sample nominal R_a roughness and measured total R_q roughness (i.e. R_q calculated based on wavelengths below 800 μm).

R_a (μm)	0.005	0.0125	0.025	0.05	0.1	0.4	1.6	3.2
R_q (μm)	0.0086	0.029	0.043	0.083	0.15	0.57	1.96	4.02

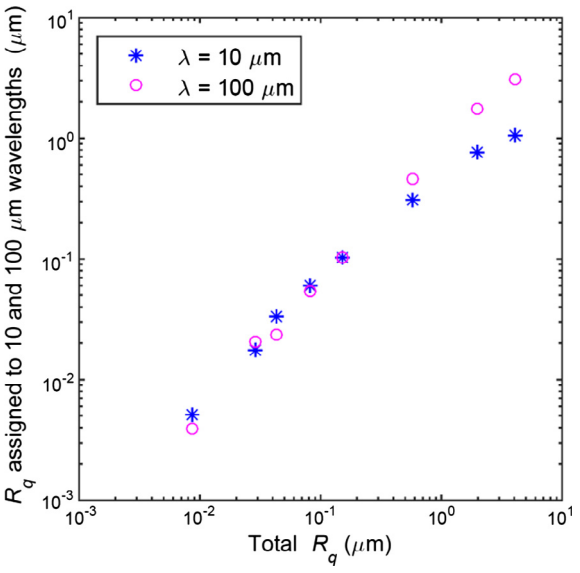

Fig. 5. Effective R_q roughness at different wavelengths (10 and 100 μm) for the different samples, as a function of total R_q. Surface spectral data was characterised with $\lambda = 10$ μm representing the range of wavelengths 3.3–33.3 μm, $\lambda = 100$ μm representing 33–333 μm wavelenths and the total R_q being based on the wavelength range 0–800 μm. (For interpretation of the references to colour in this figure legend, the reader is referred to the web version of this article.)

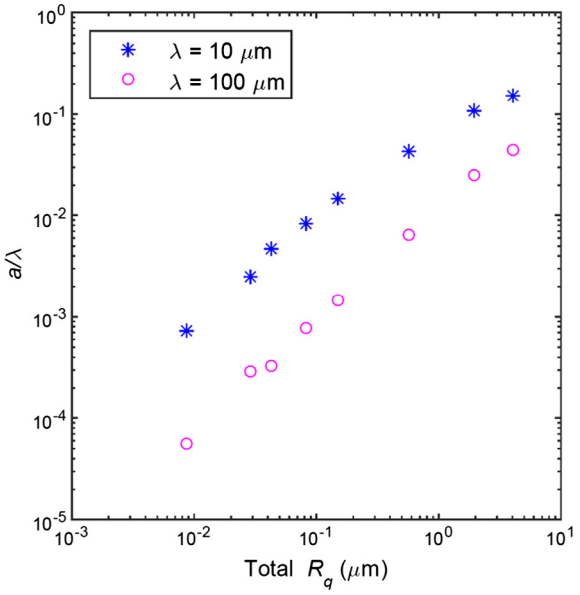

Fig. 6. Effective height to wavelength ratio a/λ (i.e. characteristic slope) for the samples with different total R_q roughness heights. (For interpretation of the references to colour in this figure legend, the reader is referred to the web version of this article.)

attributed [10] to a correspondingly higher 'real' contact area under the individual fibres. As mentioned in Section 1, this explanation has already been given some justification using an asperity modelling approach based on Hertzian contact of spherically tipped asperities on the tool surface with the cylindrical tow fibres

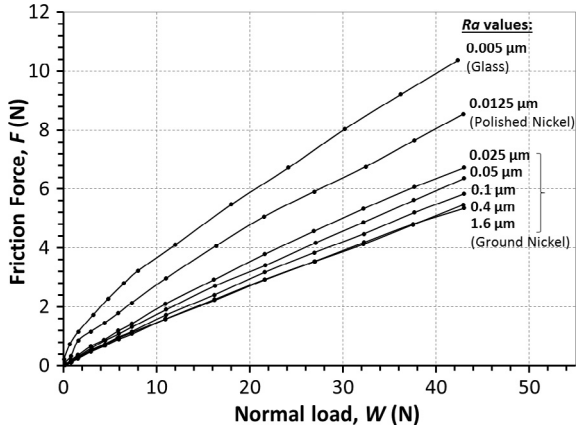

Fig. 7. Friction force versus normal load for tow in contact with surfaces with varying degrees of roughness amplitude (R_a from 0.005 to 1.6 μm). Nominal pressure at max load: 263 kPa.

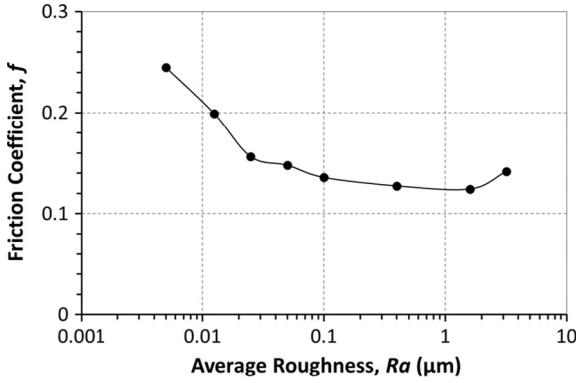

Fig. 8. Friction coefficient versus nominal average surface roughness amplitude at the highest load increment (i.e. at a nominal pressure of 263 kPa).

[2,10]. In Sections 3 and 4, however, we show how the spectral analysis of the various roughness wavelengths accompanied by an appropriate model for tow-tool contact can offer useful insight into explaining the level of tow real contact area in terms of the degree of conformance of the tow fibres with the surfaces. These sections emphasises the importance of changes in slope with roughness amplitude on the observed changes in friction.

Finally, we note that the friction force F versus normal load W curves for the various rough surfaces in Fig. 7 agree with the power law description of tow friction ($F = kW^n$) which was discussed at length from a fundamental perspective in Mulvihill et al. [5]. Table 2 shows the values of the fitting coefficients k and n for each of the surfaces tested. The value of the exponent n lies in the range 0.71–0.91, but appears to increase somewhat with surface roughness: at $R_a = 0.005$ μm, $n = 0.71$, while for $R_a = 3.2$ μm, $n = 0.91$. This change in exponent appears reasonable if we consider that increasing roughness on the counterface surfaces is likely to cause progressive departure from the ideal Hertzian cylinder-on-flat case where the exponent would be $n = 0.5$. As pointed out by Barber [18], the greater the multiscale nature of the surfaces, the more the exponent will tend to approach unity.

Table 2
Power law fitting coefficients for friction force F versus normal load W (i.e. $F = kW^n$) for the tow in contact surfaces of varying roughness.

R_a (μm)	k	n
0.005	0.72	0.71
0.0125	0.47	0.77
0.025	0.27	0.86
0.05	0.22	0.89
0.1	0.19	0.90
0.4	0.18	0.91
1.6	0.19	0.89
3.2	0.19	0.91

3. Contact mechanics modelling

This section presents a finite element (FE) idealisation of the tow-on-tool contact. The results of this analysis are used in the following section to understand the measured effect of roughness topography on friction described above. To model the tow-on-tool contact scenario illustrated in Fig. 9, we consider an idealisation akin to the Westergaard approach, as shown in Fig. 10. A rough rigid tool with a repeating sinusoidal profile of amplitude a and wavelength λ is in contact with a deformable continuum with elastic properties representing the tow. Owing to the complex anisotropic mechanical properties of the tow, an FE treatment is used. Only a region of tow of height H above the contact is modelled. The tool is modelled as a fixed rigid surface, and the tow is modelled with plane strain elastic elements. The contact between the surfaces is frictionless. Symmetry conditions are applied at the sides of the model, and the top of the model is loaded with a uniform displacement. The mean applied pressure is derived from the reaction force at the tool. The key difference between this approach and that of Cornelisson et al. [2] is that equivalent mechanical properties are used for the tow as a whole, which means that the rough counterface makes contact with a soft highly deformable body representing the fibrous assemblage rather than with cylinders having the much stiffer mechanical properties of the carbon fibres and which are constrained to remain straight.

The tow elastic properties were modelled using two element types. The transverse modulus of the tow E_t associated with compression of the tow bundle was modelled by rectangular solid elements (Abaqus element CPE4) with modulus E_t = 1 MPa and an assumed Poisson's ratio of υ_t = 0.3. The transverse modulus for the tows used in the experiments was derived from tests using the compression rig, by finding the variation in tow thickness with applied load over the range of loads applied in the friction tests.

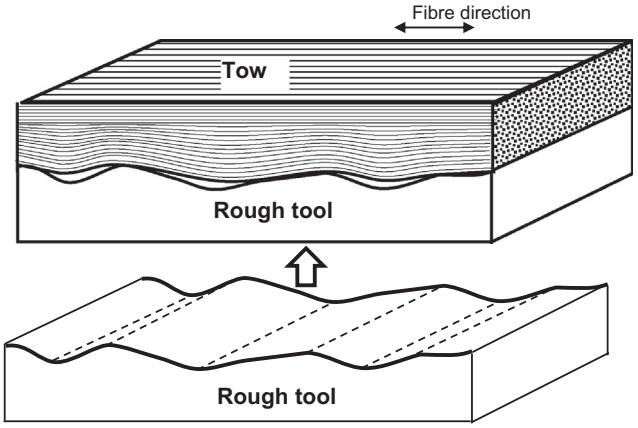

Fig. 9. Contact between a fibrous tow and a rough (ground) surface representing the tool.

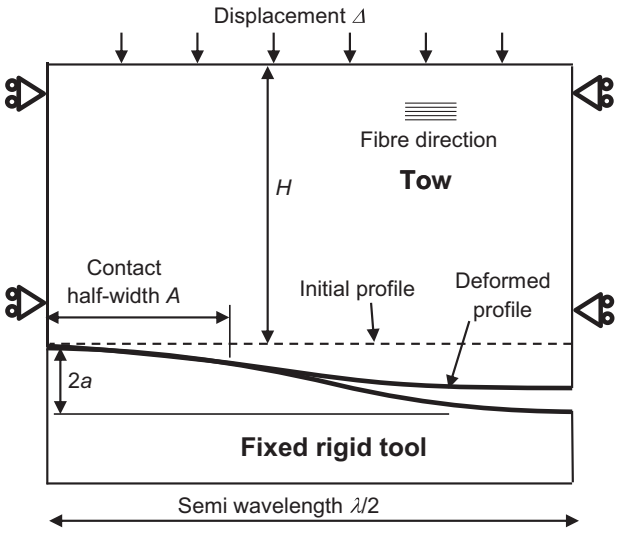

Fig. 10. Tow-tool contact idealisation for finite element modelling (i.e. deformable continuum with equivalent tow elastic properties pressing onto a rigid sinusiodal surface).

The effective modulus increased relatively gently with compressive strain after an initial compaction phase. The value chosen was appropriate to intermediate pressures applied.

The stiffness associated with fibre bending and shear was modelled using Timoshenko beam elements. Rather than modelling individual fibres, these beam elements represented a group of fibres within a given cross-sectional area of the model. For a beam element representing a cross-sectional area α, the associated fibre cross-sectional area is given by $v_f\alpha$ where v_f is the fibre volume fraction. Hence the required axial stiffness is given by $E_f v_f \alpha$, where E_f is the fibre modulus for loading along the fibre direction, taken from the manufacturer's data sheet for T700 fibres [16]. The bending stiffness B of the beam element associated with bending of the circular fibres within the cross-section is given by Liu et al. [19] as

$$B = \frac{E_f d^2}{16} \upsilon_f \alpha, \tag{3}$$

where d is the fibre diameter, taken as 7 μm from the manufacturer's data sheet [16], as confirmed from SEM measurements. Finally, the shear stiffness S of the beam is given by

$$S = kG_f \upsilon_f \alpha, \tag{4}$$

where the fibre shear modulus G_f is here assumed to be given by $E_{ft}/(2(1+\upsilon_f))$, where E_{ft} is the transverse fibre modulus and υ_f is the fibre Poisson's ratio, taken as 17 GPa and 0.31, respectively (Mounier et al. [20]). The shear factor k is taken as 0.89, appropriate to a cylindrical beam geometry (Cowper [21]). Material properties for the simulations are collected together in Table 3.

The analysis used an implicit large deformation analysis within Abaqus 6.12 [22]. A mesh refinement study was used to determine that a uniform rectangular grid of 40 elements along the length of the profile and 120 elements in the height direction was sufficient to give a converged solution. Because of the strong anisotropy of the tow, the perturbation in strains due to the surface profile extends only a very short way into the tow (c.f. the orthotropic

Table 3
Material properties used in simulation.

E_f (GPa)	G_f (GPa)	E_t (MPa)	υ_t
230	6.5	1.0	0.3

rescaling analysis of Suo et al. [23]) and a mesh height equal to 1/5 of λ was sufficient to give an accurate solution.

3.1. Finite element results

The results showed an increase in contact area with contact pressure typical of the Westergaard solution, Eq. (1). The pressure associated with significant contact (or conformance) was characterised by p^*, the pressure at which the surfaces were in complete contact. This value was extracted automatically from the Abaqus output file using Python and Matlab scripts. Fig. 11 plots the effect of the ratio a/λ of the waviness amplitude to wavelength on p^*, normalised by the transverse tow modulus E_t. Results are shown for three wavelengths $\lambda = 10$, 100 and 1000 μm. The critical pressure is approximately linearly related to a/λ, reflecting the corresponding dependence given by the Westergaard solution, Eq. (1), for the isotropic elastic solution. There is an additional strong dependence on the wavelength (comparing plots for $\lambda = 10$, 100 and 1000 μm), with longer wavelengths being deformed more easily and having a smaller p^* at a given a/λ. This dependence on wavelength, over and above the expected slope dependence, reflects the reduced bending resistance of the fibres with increasing fibre radius of curvature.

The sensitivity of the results to assumed elastic properties is assessed by taking the calculation for $a/\lambda = 0.005$, $\lambda = 100$ μm, and doubling in turn the assumed values of E_f, E_t and G_f. These increases in E_f, E_t and G_f result in increases in p^* of 56%, 14% and 25%, respectively. Results show the greatest sensitivity to E_f, emphasising the important role of fibre bending stiffness. Reducing the tow Poisson's ratio υ_t from 0.3 to 0.15 results in a 3% drop in p^*, demonstrating relative insensitivity to this parameter. For the same case, the Westergaard model for an isotropic elastic solid would give the same value of p^* as the FE tow model by taking a value of $E^* = 118$ MPa. That this value is neither near the transverse modulus E_t of 1 MPa nor the fibre modulus E_f of 230 GPa confirms the need for the more sophisticated elastic model undertaken here.

4. Application of modelling to experiments and discussion

The above FE calculations provide a way of understanding the likely contact and hence friction behaviour in the experiments with rough surfaces. For a given roughness geometry, first the characteristic slopes a/λ at 10 and 100 μm wavelengths can be found from Fig. 6. Fig. 11 then gives the corresponding pressure p^* for complete contact for these wavelengths of roughness, using the quadratic fit to the data shown as solid lines in this plot to extrapolate beyond the range of the calculations. Where the applied pressure falls below p^* then the contact area ratio $2A/\lambda$ is assumed to be given by Eq. (1) (an assumption which the FE results confirm is reasonable). The final element in the analysis is to treat the problem as a two-scale contact. The average pressure at the 100 μm length scale is taken equal to the applied nominal pressure, to first allow calculation of the corresponding contact ratio $(2A/\lambda)_{100}$ for this length scale. Now the 10 μm roughness analysis applies, but only to those parts of the 100 μm roughness found to be in contact. The nominal pressure on these shorter wavelength asperities equals the overall nominal pressure divided by the contact ratio $(2A/\lambda)_{100}$.

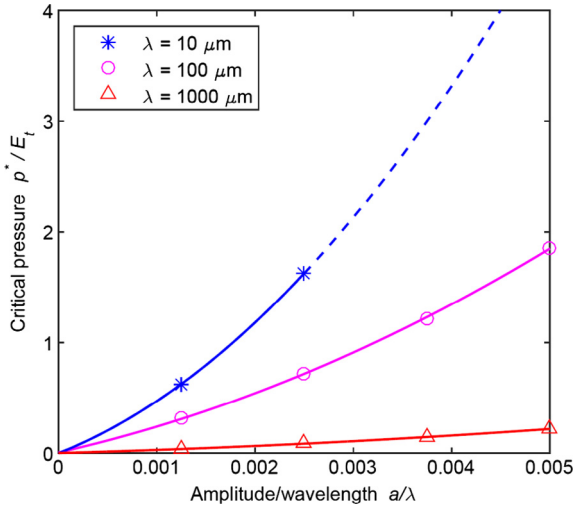

Fig. 11. Effect of height to wavelength ratio a/λ (i.e. charateristic slope) and roughness wavelength λ on p^*/E_t, the critical contact pressure required to give complete contact normalised by the tow transverse stiffness. The dashed part of the line for $\lambda = 10$ μm is an extrapolation of a quadratic fit to the data (the solid lines in each case). (For interpretation of the references to colour in this figure legend, the reader is referred to the web version of this article.)

The results of the above calculations are detailed in Table 4 for a nominal pressure equal to the maximum value used of 263 MPa. Each line in the table corresponds to a different roughness amplitude. The contact ratios $2A/\lambda$ at 100 and 10 μm length scales are included towards the right of the table. For the smoothest surface, the slopes are sufficiently small that complete conformance is predicted for the 100 μm scale of roughness and 67% contact is predicted for the 10 μm scale roughness. Hence, for this smoothest surface, conditions between the fibres and rough surface tend to those of a line contact. This prediction is confirmed by observations of the fibre contact with glass surfaces, which show such a line contact behaviour [5,7]. However, as the R_a amplitude and slope increases, the contact ratio of the small scale roughness decreases to a value of 0.1 for an R_a of 0.05 μm. For this case the contact length between the fibre and tool at this length scale is only 1 μm, significantly less than the fibre diameter. Contact between the fibre and tool is now close to point contact conditions. For roughness amplitudes of 0.1 μm and above, the predicted critical pressures for complete conformance are greater than 20 times the tow transverse modulus, and use of the extrapolated FE calculations to predict contact conditions becomes increasingly unreliable. Nevertheless it is expected that point contact conditions continue to pertain for these rougher surfaces. It is important to note that the critical factor in the transition from line to point contact is associated with the shorter wavelength roughness, which has higher slopes and which brings into play fibre bending stiffness.

The friction coefficient results at a nominal pressure of 263 kPa, given in Fig. 8 and the final column of Table 4, have a similar transition in behaviour from the smooth surface result with relatively high friction to a friction coefficient for the rougher surfaces close to the friction coefficient of 0.13 observed for crossed tows with effectively point contact conditions [5]. Mirroring the predictions of contact geometry changes from line to point contact, there is a sharp change in friction for roughness amplitudes between 0.005 and 0.05 μm, but little change for surfaces rougher than 0.05 μm. This comparison supports the notion that the FE model captures reasonably well the physical phenomenon controlling friction, i.e. the change in fibre conformance with roughness topography changes conditions at the contact from line to point contact. Although qualitively helpful, a more sophisticated model would be needed to make accurate quantitative predictions of friction, including the three-dimensional geometry of the contacts and the way that, at small contact pressures, only a small fraction of the fibres in a given region make contact with the tool surface [5,7].

The friction results of Figs. 7 and 8 include contact between fibres and either glass, for the smoothest surface, or nickel for the roughened surfaces. It might be expected that changes in the counterface material would significantly affect friction. However

Table 4
Application of FE calculations to experimental measurements at a nominal pressure of 263 kPa.

R_a (μm)	Slope a/λ		p^*/E_t		Contact ratio $2A/\lambda$		Contact	Friction coefficient
	λ = 100 μm	λ = 10 μm	λ = 100 μm	λ = 10 μm	λ = 100 μm	λ = 10 μm		
0.005	5.5×10^{-5}	7.8×10^{-4}	0.017	0.35	1	0.67	Tending to line	0.24
0.0125	2.9×10^{-4}	0.0025	0.067	1.6	1	0.26	Transition	0.20
0.025	3.3×10^{-4}	0.0048	0.076	4.4	1	0.16	Transition	0.16
0.05	7.6×10^{-4}	0.0084	0.18	11	1	0.10	Point	0.15
0.1	0.0014	0.015	0.35	>20	0.66	<0.1	Point	0.14
0.4	0.0065	0.043	2.7	>20	0.20	<0.1	Point	0.13
1.6	0.025	0.11	>20	>20	<0.1	<0.1	Point	0.12
3.2	0.044	0.15	>20	>20	<0.1	<0.1	Point	0.14

the results for the glass are in line with the results for the nickel, suggesting that, in fact, the counterface material is not critical. Instead it is supposed, following the inference in [5], that the interfacial strength and hence friction is determined by the strength of the sizing on the fibres rather than the counterface material.

The above results highlight the importance of the slope and wavelength in determining the extent to which the composite fibres can conform to the tool surface and hence change the contact mode from line to point contact. It is expected that the fibres (for anisotropic surfaces) would conform relatively easily to the roughness in the direction parallel to the surface machining marks. The important characteristic of the tool roughness is, therefore, its variation along the fibre direction, and more specifically the wavelength and slope in this direction.

The importance of fibre bending seen in the results of Fig. 11 suggest that fibre diameter could be expected to influence significantly the friction behaviour, with larger diameter fibres being stiffer in bending and hence tending to lead to lower-friction point contact behaviour.

5. Conclusions

A comprehensive experimental study of the effect of tool surface roughness topography on tow-on-tool friction has been carried out. Friction force F versus normal load W curves were recorded for carbon fibre tows in contact with counterface surfaces having a wide range of average surface roughness R_a values from 0.005 to 3.2 μm. The slopes of these surfaces, which play the critical important role in the contact behaviour, increased in line with the roughness amplitudes. All F-W curves obeyed the power law description $F = kW^n$ with the exponent n being in the range 0.71–0.91 and tending to increase with increasing roughness amplitude and slope. Friction was found to increase rapidly with decreasing surface roughness and slope for surfaces having an R_a less than about 0.1 μm, but was relatively insensitive to roughness for higher R_a values. A finite element based contact modelling approach was used to explain these results in terms of the level of tow conformance with the counterface surfaces. The smoother low-slope surfaces allowed the tows to conform well to the surfaces and, hence, generate a higher real contact area and a friction force more sensitive to changes in roughness, while the rougher high-slope surfaces showed poor conformance allowing the peaks of the roughness profile to dominate the contact causing the real contact area under the fibres (and hence, the friction) to be less sensitive to roughness.

Acknowledgements

The authors would like to acknowledge the assistance of the Engineering and Physical Sciences Research Council (EPSRC) for supporting the present work under grant Ref. EP/K032798/1 (Friction in Composites Forming). We would also like to acknowledge the contribution of our industrial collaborators at Jaguar Land Rover and Granta Design Ltd, as well as our academic partners from the Composites Research Group at the University of Nottingham (Prof. Andy Long, Prof. Nick Warrior and Prof. Davide De Focatiis). Dr Olga Smerdova of "Institut PPrime", ISAE-ENSMA, Poitiers is thanked for useful discussions throughout the work. Hexcel are thanked for supplying the tow material. Data relating to this paper are available at the following Cambridge University data repository: http://dx.doi.org/10.17863/CAM.6075.

References

[1] Cornelissen B, de Rooij MB, Rietman B, Akkerman R. Frictional behavior of carbon fiber tows: a contact mechanics model of tow–tow friction. Text Res J 2014;84(14):1476–88.
[2] Cornelissen B, de Rooij MB, Rietman B, Akkerman R. Frictional behaviour of high performance fibrous tows: a contact mechanics model of tow–metal friction. Wear 2013;305(1–2):78–88.
[3] Cornelissen B, Rietman B, Akkerman R. Frictional behaviour of high performance fibrous tows: friction experiments. Compos A Appl Sci Manuf 2013;44:95–104.
[4] Chakladar ND, Mandal P, Potluri P. Effects of inter-tow angle and tow size on carbon fibre friction. Compos A Appl Sci Manuf 2014;65:115–24.
[5] Mulvihill DM, Smerdova O, Sutcliffe MPF. Friction of carbon fibre tows. Compos A: Appl Sci Manuf 2017 [in press].
[6] Smerdova O, Sutcliffe MPF. Novel experimental method for microscale contact analysis in composite fabric forming. Exp Mech 2015;55(8):1475–83.
[7] Smerdova O, Sutcliffe MPF. Multiscale tool–fabric contact observation and analysis for composite fabric forming. Compos A Appl Sci Manuf 2015;73:116–24.
[8] Greenwood JA, Williamson JBP. Contact of nominally flat surfaces. Proc Roy Soc Lond. Ser A Math Phys Sci 1966;295(1442):300–19.
[9] Bowden FP, Tabor D. The friction and lubrication of solids. Oxford: Clarendon Press; 1950.
[10] Roselman IC, Tabor D. The friction and wear of individual carbon fibres. J Phys D Appl Phys 1977;10(8):1181.
[11] Johnson KL. Contact mechanics. Cambridge (UK): Cambridge University Press; 2003.
[12] Mulvihill DM, Kartal ME, Nowell D, Hills DA. An elastic–plastic asperity interaction model for sliding friction. Tribol Int 2011;44(12):1679–94.
[13] Mulvihill DM, Brunskill H, Kartal ME, Dwyer-Joyce RS, Nowell D. A comparison of contact stiffness measurements obtained by the digital image correlation and ultrasound techniques. Exp Mech 2013;53(7):1245–63.
[14] Westergaard HM. Bearing pressures and cracks. Trans ASME J Appl Mech 1939;6(49):399.
[15] Persson BNJ. Theory of rubber friction and contact mechanics. J Chem Phys 2001;115(8):3840–61.
[16] Torayca T700S datasheet. Technical datasheet No. CFA-005. Torayca Carbon Fibers Inc. Santa Ana, CA, USA. <http://www.toraycfa.com/pdfs/T700SDataSheet.pdf>.
[17] Stoica P, Moses R. Introduction to spectral analysis. Prentice-Hall; 1997.
[18] Barber JR. Multiscale surfaces and Amontons' law of friction. Tribol Lett 2013;49(3):539–43.
[19] Liu D, Fleck NA, Sutcliffe MPF. Compressive strength of fibre composites with random fibre waviness. J Mech Phys Solids 2004;52(7):1481–505.
[20] Mounier D, Poilâne C, Bûcher C, Picart P. Evaluation of transverse elastic properties of fibers used in composite materials by laser resonant ultrasound spectroscopy. Société Française d'Acoustique. Acoustics 2012, Nantes, France; 2012.
[21] Cowper GR. The shear coefficient in Timoshenko's beam theory. J Appl Mech 1966;33(2):335–40.
[22] ABAQUS User's Manual v6.12. Dassault Systemes Simula Corporation. RI (USA): Providence; 2012.
[23] Suo Z, Bao G, Fan B, Wang TC. Orthotropy rescaling and implications for fracture in composites. Int J Solids Struct 1991;28(2):235–48.